https://doi.org/10.3311/PPch.42428
Creative Commons Attribution

Periodica Polytechnica Chemical Engineering

Synthesis of Porous ZnO Photocatalyst Using Carbon Microsphere Template for Methylene Blue Degradation

Ilyas Taufik Abdul Aziz[1*], Mohammad Jihad Madiabu[1], Supriyono Supriyono[1], Arie Pratama Putra[1], Anom Cahyotomo[1], Hanum Sekar Panglipur[1], Dicky Annas[2]

[1] Chemical Analysis Study Program, Politeknik AKA Bogor, Pangeran Sogiri 283, 16154 Bogor, Indonesia
[2] Research Center for Catalysis, National Research and Innovation Agency (BRIN), B.J. Habibie Science and Technology Area, 15314 South Tangerang, Indonesia
[*] Corresponding author, e-mail: ilyastaufik@aka.ac.id

Received: 07 October 2025, Accepted: 02 February 2026, Published online: 25 February 2026

Abstract

Porous zinc oxide photocatalysts were successfully synthesized using carbon microsphere templating method. This study investigated the effect of carbon microsphere templates on the physicochemical properties and photocatalytic performance of ZnO in methylene blue degradation. Carbon microspheres were prepared via hydrothermal method and subsequently used as templates to obtain porous ZnO through wet impregnation route. The carbon templates exhibited a uniform spherical morphology with an average diameter of less than 1 μm and an amorphous structure, while the resulting ZnO showed a highly porous structure with good crystallinity, surface area of 9 $m^2\ g^{-1}$, total pore volume of 0.034 $cm^3\ g^{-1}$, pore size of 5.9 nm and a band gap of 3.17 eV. Photocatalytic tests revealed that ZnO degradation efficiency increased with UV irradiation time, reaching the highest value of 39.3 ± 0.2% at 150 min, and the reaction followed first-order kinetics with a rate constant of 0.0032 ± 0.0001 min^{-1}. These results explained that carbon template-assisted synthesis is a powerful, tunable approach for tailoring ZnO structure and provides a basis for developing a photocatalyst for environmental applications.

Keywords

methylene blue, porous, photocatalyst, zinc oxide

1 Introduction

Methylene blue or 3,7-bis(dimethylamino)phenothiazin-5-ium chloride or methylthioninium chloride is an organic dye widely used in the textile, pharmaceutical, cosmetic, food and printing industries [1, 2]. Despite its widespread application, methylene blue exhibits toxic, carcinogenic, mutagenic, stable, and non-biodegradable properties, thereby posing serious risks to human health and the environment [3]. However, due to its distinct spectroscopic characteristic, stability and easily monitored, this compound commonly used as model pollutant in some research, particularly in photocatalysis research [4]. Based on this condition, the removal of methylene blue becomes a challenge. Various methods have been developed to remove methylene blue from the environment, such as biological treatment using enzymes and microorganisms, adsorption, coagulation, filtration and advanced oxidation processes [5]. Nowadays, the photocatalysis process has gained significant attention due to its environmental friendliness, efficiency, low cost and lack of secondary pollutants [6].

The photocatalysis method requires semiconductor materials (photocatalyst) to facilitate and accelerate photochemical reactions [7]. Metal oxides such as ZnO, CuO, CeO, NiO, WO_3, TiO_2, SnO_2 and Al_2O_3 have been studied as photocatalyst [8, 9]. ZnO is considered superior because of its wide bandgap (3.37 eV), high electron mobility, thermal and chemical stability, high photosensitivity, low cost, environmentally friendly and easy preparation [10, 11]. The photocatalytic performance of ZnO depends on several factors, including its morphology [12]. The morphology of ZnO relates to its cross-sectional and surface areas, which consequently affect the material's faces exposed to light, thereby influencing their photocatalytic performance [13]. Various ZnO morphologies have been synthesized, including nanotubes, nanowires, nanorods, nanobelts and nanosheets [14]. Among the

Cite this article as: Aziz, I. T. A., Madiabu, M. J., Supriyono, S., Putra, A. P., Cahyotomo, A., Sekar Panglipur, H., Annas, D. "Synthesis of Porous ZnO Photocatalyst Using Carbon Microsphere Template for Methylene Blue Degradation", Periodica Polytechnica Chemical Engineering, 2026. https://doi.org/10.3311/PPch.42428

various morphologies of ZnO porous nanostructures are favorable for numerous applications because of their high specific surface area [15].

Several methods have been developed to synthesize porous materials, including soft and hard template methods, electrochemical anodization, and direct assembly [16]. Among the available techniques hard templating offers some advantages such as higher stability, better control of size and morphology and good feasibility [17]. The choice of template is a critical factor in hard template synthesis methods [18]. In practice, there are several types of templates such as mesoporous silica template, carbon template and metal organic framework polymer template [18]. Between the existing template, carbon microspheres have several advantages such as being environmentally friendly and energy efficient [19]. In principle, the formation of the carbon microsphere structure occurs by the sequential reduction of carbohydrates under solvothermal conditions [20]. The environmentally friendly nature of carbon microspheres enhances their value as templates for synthesizing porous ZnO. Research on porous ZnO synthesized via carbon microsphere templates for methylene blue degradation remains limited. Hence, this study focused on synthesizing and characterizing porous ZnO using carbon microsphere template and evaluating its photocatalytic performance in methylene blue degradation.

2 Materials and methods

2.1 Materials

The materials used in this research consisted of fructose (Merck), ethanol (Sigma Aldrich), zinc nitrate tetrahydrate ($Zn(NO_3)_2 \cdot 4H_2O$; Sigma Aldrich), methylene blue (Merck), and distilled water. All chemicals were p.a. (pro analysis) reagents and used without further purification.

2.2 Methods

2.2.1 Synthesis carbon microsphere template

Carbon microspheres were synthesized via hydrothermal method. 8.7 g of fructose was dissolved in 100 mL of distilled water and transferred into teflon-lined stainless steel autoclave (200 mL, Alish Tech, Indonesia). The autoclave was sealed and heated at 180 °C for 4 h. The resulting suspension was cooled to room temperature, followed by centrifugation. The obtained solid was washed with distilled water and ethanol several times. The solid product was dried at 80 °C overnight and continued with grinding.

2.2.2 Synthesis of porous ZnO

2 g $Zn(NO_3)_2 \cdot 4H_2O$ was dissolved in 40 mL of distilled water and 1 g carbon microsphere was dispersed in 20 mL distilled water. The two solutions were mixed and stirred at room temperature for 5 h, followed by aging for 24 h. The mixture was centrifuged and the solid product was washed several times with distilled water. The product was calcined at 500 °C for 2 h. The resulting white solid was cooled to room temperature. ZnO was also synthesized without using carbon microsphere template (ZnO Ref) for comparison.

2.2.3 Evaluation of the photocatalytic performance of porous ZnO

A series of photocatalytic studies was conducted to evaluate the photocatalytic performance of porous ZnO for methylene blue degradation. The first step was the preparation of 100 mg L^{-1} methylene blue stock solution. The second step was preparation of standard calibration curve by diluting methylene blue stock solutions to 0, 1, 2, 3, 4, and 5 mg L^{-1}, followed by absorbance measurement.

Photocatalytic degradation efficiency of porous ZnO was evaluated by adding 25 mg porous ZnO into 50 mL of 5 mg L^{-1} methylene blue solution. The mixture was stirred in dark place for 30 min to ensure uniform dispersion. This dark period time refers to research conducted by Wang et al. [21]. After that, the mixture was placed into UV reactor and irradiated for 30, 60, 90, 120, and 150 min. The absorbance of the solutions was measured using a UV-Vis spectrophotometer (PharmaSpec UV-1700, Japan), and their concentration was determined. The photocatalytic degradation efficiency tests were conducted in triplicate. The control solution was analyzed under the same conditions, but without catalyst. The degradation efficiency of porous ZnO catalyst for methylene blue degradation was calculated using Eq. (1) [22]:

$$\text{Degradation efficiency } (\%) = \frac{C_0 - C_t}{C_0} \times 100\% \quad (1)$$

where C_0 is the initial concentration of the methylene blue solution and C_t is the concentration after irradiation for t min.

The kinetic rate constant of methylene blue degradation with porous ZnO was determined using first-order rate equation [23]. The rate constant was calculated with Eq. (2):

$$\ln \frac{C_0}{C_t} = k \times t \quad (2)$$

where k is degradation rate constant (min^{-1}), and t is the irradiation time. The reaction rate constant was obtained by finding the gradient of the $\ln\frac{C_0}{C_t}$ vs. t plot.

3 Results and discussion

3.1 Carbon microspheres

3.1.1 Fourier transform infrared characterization

Carbon microspheres were characterized by Fourier transform infrared (FTIR; Bruker Alpha, Germany) to determine the functional group present in the material. The result is depicted in Fig. 1.

The FTIR spectrum of the carbon microspheres shows a broad band at 3340 cm^{-1} corresponding to the O–H stretching vibration of the carboxylate group. The band at 2920 cm^{-1} is attributed to the asymmetric C–H stretching vibration of the aliphatic group. The strong band at 1662 cm^{-1} represents the C=O stretching vibration, whereas the band at 1514 cm^{-1} is the characteristic band of pentagonal heteroaromatic rings. The bands in the range 964–1190 cm^{-1} region are assigned to C–O stretching vibration and O–H bending. The band at 766 cm^{-1} indicates the wagging vibration of hydrogen adsorbed on the pentagon ring with an unsubstituted CH=CH group [24–26]. Oxygen-containing functional groups on carbon microspheres such as hydroxyl, carbonyl, and carboxyl act as coordination sites for Zn^{2+} ions (ZnO precursor) during the synthesis [27]. These interactions influence the formation of the porous structure in ZnO after calcination.

3.1.2 Characterization by X-ray diffraction

The X-ray diffraction (XRD) was performed on an X-ray diffractometer (Bruker D2 Phaser, Germany). The diffractogram of carbon microsphere is depicted in Fig. 2.

The diffractogram shows a broad peak at $2\theta = 23°$, indicating the (002) plane of hexagonal lattice diffraction of graphite with amorphous structure [28]. The crystallite size was calculated using the Debye-Scherrer equation [29], and the result was 0.78 nm.

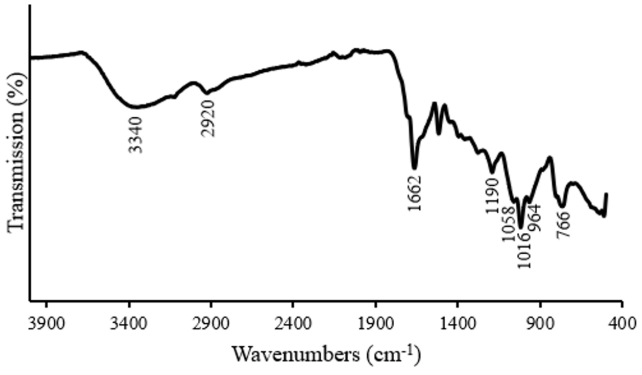

Fig. 1 FTIR spectrum of carbon microspheres

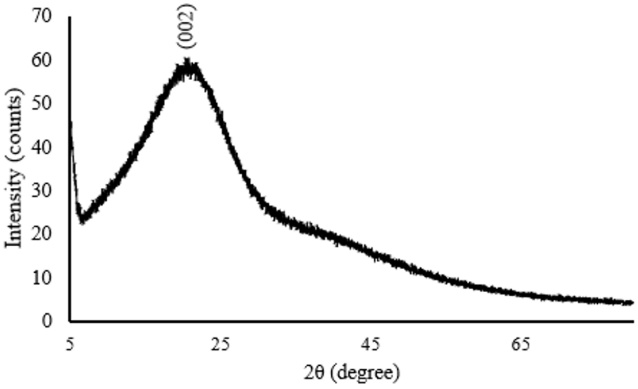

Fig. 2 Diffractogram of carbon microsphere

3.1.3 Characterization by scanning electron microscopy

Scanning electron microscopy (SEM) characterization was performed using scanning electron microscope (JSM-6510LA, JEOL Ltd., Japan) to investigate the morphological appearance of the synthesized carbon microspheres. SEM image of carbon microsphere at 10000× magnification is shown in Fig. 3.

Based on the SEM results, the carbon microspheres have uniform spherical morphology with a smooth surface and an average diameter of less than 1 μm. Moreover, the SEM image displayed that the existing spherical particles are well dispersed. The uniform spherical shape facilitates homogeneous coating or adsorption of Zn^{2+} ions during the precursor impregnation, leading to more controlled nucleation of ZnO. Additionally, the good dispersion of the spheres helps ensure the uniform template distribution throughout the precursor matrix, which contributes to the formation of a porous ZnO network after calcination.

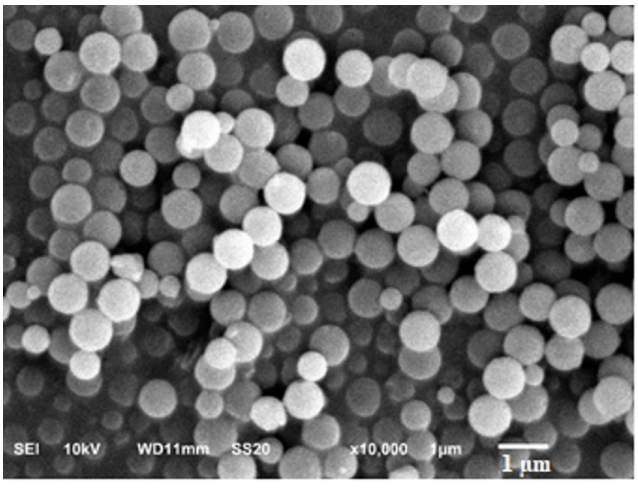

Fig. 3 Carbon microsphere SEM image

3.2 Porous ZnO

3.2.1 Fourier transform infrared characterization

The FTIR characterization was performed to determine the functional groups in porous ZnO and evaluate the impact of the carbon microsphere template in ZnO synthesis, particularly regarding the wavenumber shifts. FTIR spectra of ZnO Ref and porous ZnO are depicted in Fig. 4.

The FTIR spectra of ZnO Ref and porous ZnO exhibit distortion in the low wavenumber region; however, peaks at 418–470 cm^{-1} and 428–484 cm^{-1}, which correspond to the Zn–O stretching vibration, are still observed [20]. The FTIR spectra show that the Zn–O absorption band in porous ZnO appears at a higher wavenumber than in ZnO Ref, which may be attributed to residual carbon in porous ZnO. Carbon is a lighter atom than Zn, causing the Zn–O bond stretching frequency shifting to higher value [30, 31].

3.2.2 XRD characterization

XRD characterization was performed to determine the crystallinity of the materials and assess the effect of carbon microsphere modification on ZnO. The diffractograms of ZnO Ref and porous ZnO are shown in Fig. 5.

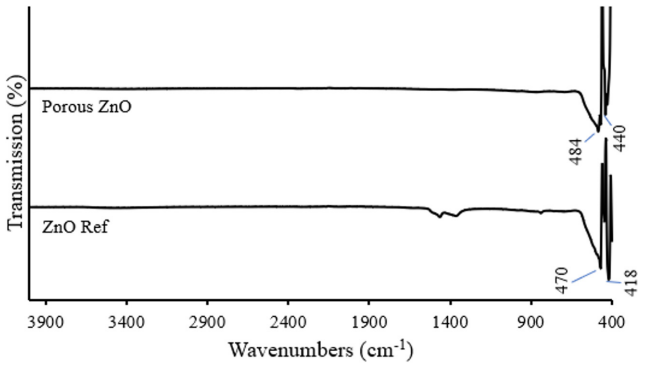

Fig. 4 FTIR spectra of ZnO Ref and porous Zn

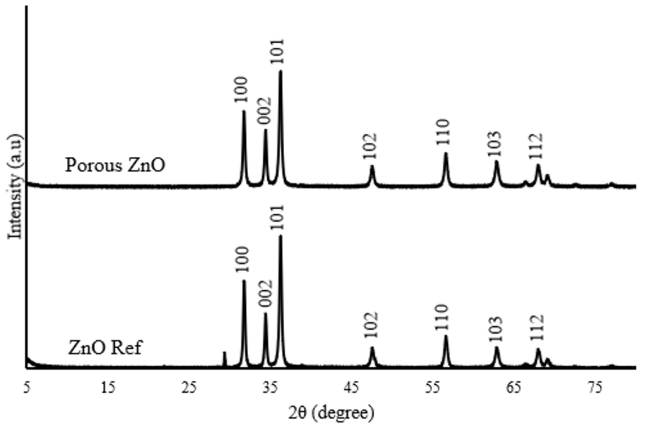

Fig. 5 Diffractogram of ZnO Ref and porous ZnO

The diffractograms of ZnO Ref and porous ZnO display several sharp peaks, confirming that both materials possess a structure with a high degree of crystallinity. The peaks appear at 2θ = 31.79; 34.43; 36.26; 47.56; 56.61; 62.87; 67.96 for ZnO Ref and 31.77; 34.42; 36.25; 47.54; 56.60; 62.85; 67.95 for porous ZnO. According to JCPDS no. 36-1451, these peaks correspond to the hexagonal wurtzite phase of ZnO, associated with (100), (002), (101), (102), (110), (103), and (112) lattice planes [32]. ZnO Ref and porous ZnO show no significant difference, indicating that the modification with carbon microspheres does not significantly alter the crystal structure of ZnO. The crystallite sizes from three main peaks were calculated using Debye-Scherrer equation, and the results are summarized in Table 1.

Table 1 shows that the crystallite size of porous ZnO is smaller than of ZnO Ref. These results indicate that employing carbon microsphere templates in ZnO synthesis reduces the crystallite size.

3.2.3 SEM-EDX mapping

Scanning electron microscopy coupled with energy dispersive X-ray spectroscopy (SEM-EDX) mapping was performed performed using scanning electron microscope (JSM-6510LA, JEOL Ltd., Japan) to examine the morphological appearance, elemental composition and elemental distribution of porous ZnO. The SEM characterization result of porous ZnO at 10000× magnification is presented in Fig. 6.

SEM analysis confirms that the ZnO modified with carbon microspheres has porous morphology with varying size of cavities. The thermal decomposition of the carbon template leaves behind hollow regions, resulting in a porous architecture. The results of the EDX and mapping analysis of porous ZnO are listed in Table 2 and Fig. 7, respectively.

EDX analysis exhibits that the composition of Zn and O on porous ZnO are 83.40 and 16.60 mass%, respectively. The mapping results indicate that the Zn and O elements are equally distributed on the material's surface.

Table 1 Crystallite size of ZnO Ref and porous ZnO

Sample	Lattice plane	Crystal size (nm)
ZnO Ref	(100)	33.51
	(002)	34.81
	(101)	30.69
Porous ZnO	(100)	32.83
	(002)	33.17
	(101)	28.97

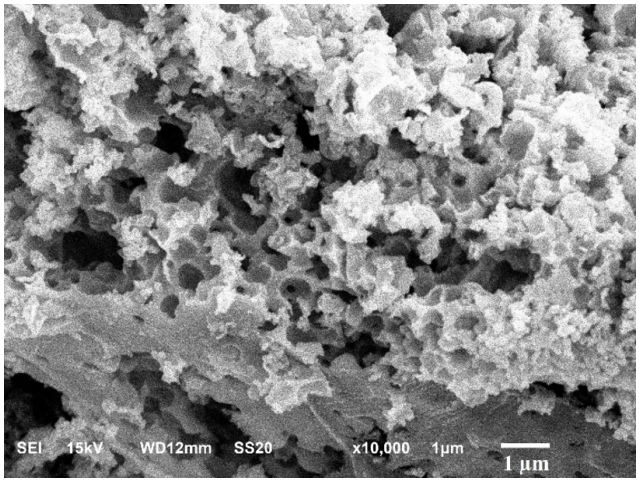

Fig. 6 SEM image of porous ZnO

Table 2 EDX result of porous ZnO

Element	Mass %	Atom %
Zn	83.40	55.14
O	16.60	44.86

3.2.4 Surface area and porosity

The specific surface area, total pore volume and pore size of materials are tabulated in Table 3. The measurements were carried out using Surface Area and Porosity Analyzer (Micromeritics Tristar II 3020, USA) employing N_2 as the probe gas and temperature of the measurement −196 °C. Brunauer-Emmett-Teller (BET) model was applied to determine the specific surface area (A), while the Barrett-Joyner-Halenda (BJH) based on desorption branch of the isoterm method was used to calculate total pore volume. The pore size (D) was calculated from BJH desorption data using relationship $D = 4V/A$, where V is the total pore volume.

This characterization shows that the ZnO prepared using carbon sphere template exhibits higher surface area, total pore volume, and pore size than ZnO Ref. A larger pore size enhances the diffusion rate of adsorbate in materials, while a higher surface area and pore volume increase the adsorption capacity for adsorbate [33, 34].

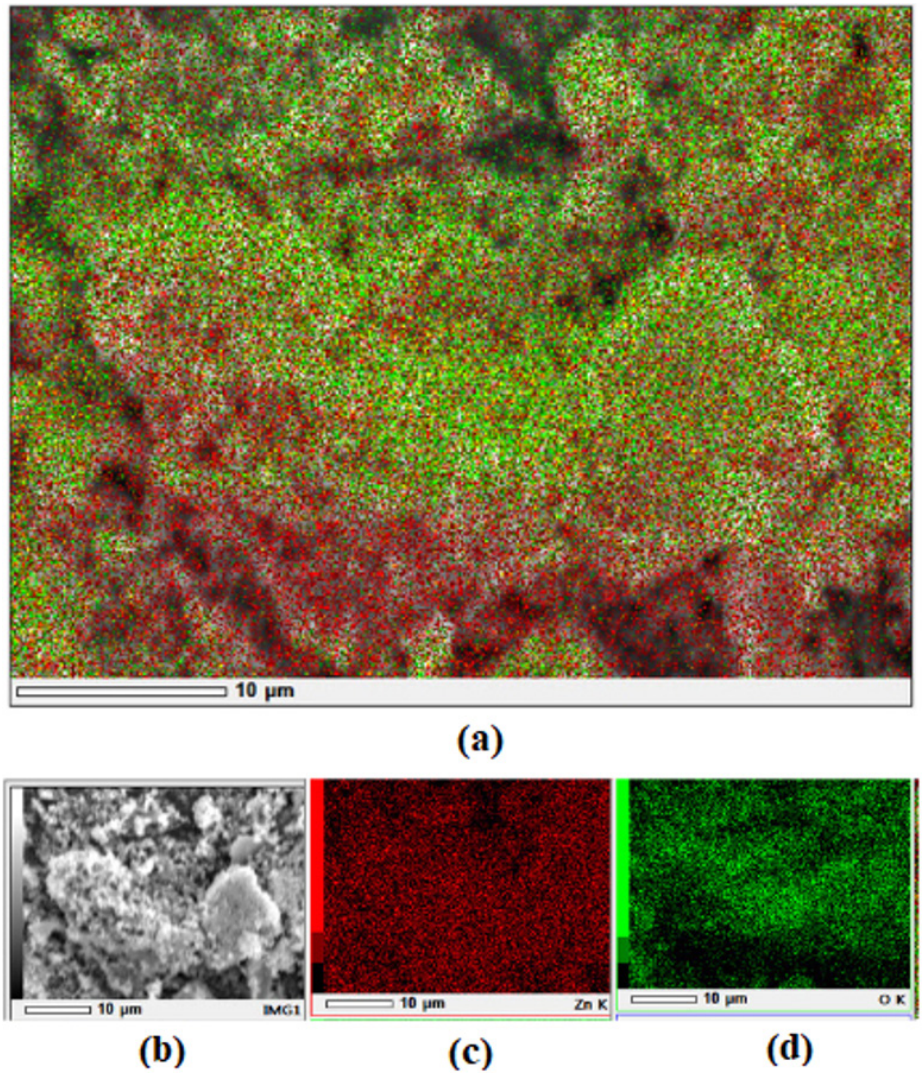

Fig. 7 SEM image and elemental mapping of porous ZnO: (a) Zn and O elemental map, (b) SEM image, (c) Zn elemental map, and (d) O elemental map

Table 3 Surface area and porosity characterization result

Materials	Specific surface area ($m^2\ g^{-1}$)	Total pore volume ($cm^3\ g^{-1}$)	Pore size (nm)
ZnO Ref	3	0.008	4.2
Porous ZnO	9	0.034	5.9

3.2.5 UV-Vis diffuse reflectance spectroscopy analysis

UV-Vis diffuse reflectance spectroscopy (DRS) characterization was performed using UV-Vis Spectrophotometer (Analytik Jena Specord 200 Plus, Germany) to determine the bandgap energy values of ZnO Ref and porous ZnO. The UV-Vis DRS spectra of ZnO Ref and porous ZnO are depicted in Fig. 8.

The reflectance values were used to determine the indirect bandgap using the Kubelka-Munk equation [35]. The bandgap value of ZnO Ref and porous ZnO were obtained by plotting the square of the Kubelka-Munk function ($F(R)^2$) against bandgap energy *Eg* as shown in Fig. 9.

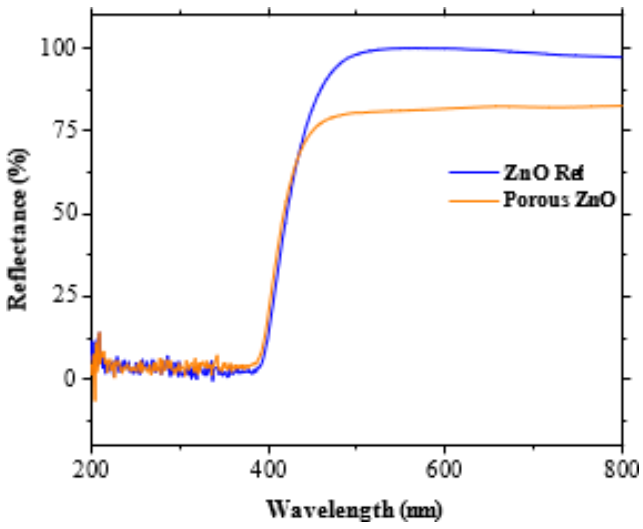

Fig. 8 UV-Vis DRS spectra of ZnO Ref and porous ZnO

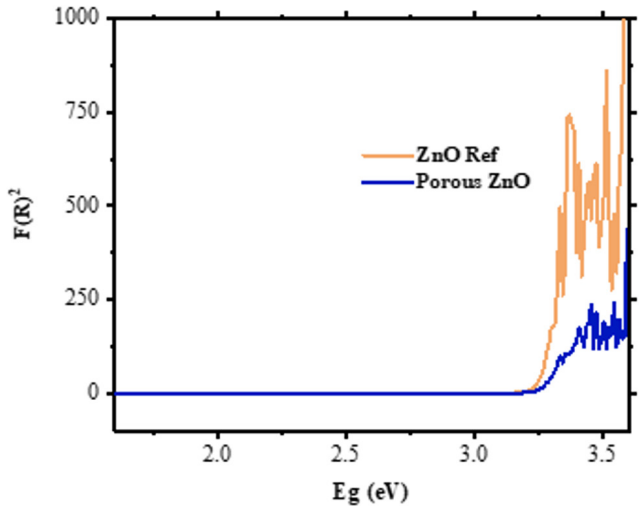

Fig. 9 Indirect bandgap plot of ZnO Ref and porous ZnO

The bandgap value of ZnO Ref and porous ZnO derived from the plot are listed in Table 4.

Table 4 shows that porous ZnO has bandgap value of 3.17 eV which indicates that this material is active under UV light. Moreover, porous ZnO has a slightly smaller bandgap value than ZnO Ref. The change in bandgap value may be attributed to crystal defects in porous ZnO as a result of structural modification with carbon microspheres [36]. Reducing the band gap value generally increases the light absorption and electron excitation capabilities, which can help improve photocatalytic activity [37].

3.2.6 Photocatalytic performance test of porous ZnO

The results of the degradation efficiency test of methylene blue using porous ZnO catalyst and without catalyst (standard) at different times are presented in Fig. 10.

Fig. 10 shows that the degradation efficiency increases with longer irradiation time when porous ZnO catalyst is used as catalyst. In this study, no measurable signal detected during dark period and the highest degradation efficiency of porous ZnO (39.3%) was obtained at 150 min of irradiation and the kinetic study shows that the kinetic constant value of methylene blue degradation with porous ZnO catalyst under UV irradiation conditions is $0.0032 \pm 0.0001\ min^{-1}$. The comparison of methylene blue degradation efficiency between this research and the other research listed in Table 5 [38–41].

This comparison highlights that the porous ZnO exhibits low catalytic performance. This result can be attributed to its wide band gap of 3.17 eV, which restricts light absorption to a narrow UV region and thereby limits the number of photons available to drive photocatalytic

Table 4 Bandgap values of ZnO Ref and porous ZnO

Materials	Bandgap value (eV)
ZnO Ref	3.20
Porous ZnO	3.17

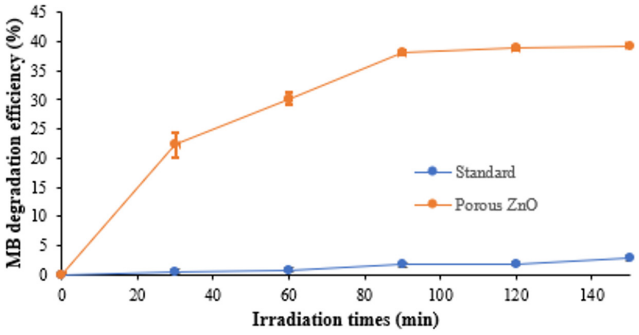

Fig. 10 Degradation efficiency of methylene blue (MB) with porous ZnO and without (standard)

Table 5 Comparison of methylene blue degradation efficiency and rate constant of ZnO photocatalyst

Catalyst	Light source	Radiation time (min)	Degradation efficiency (%)	Reference
Porous ZnO synthesized with carbon microsphere template	UV radiation	150	39.3	This work
Porous ZnO	Light Emitted Diode	120	2.5	[38]
ZnO nanoparticle prepared by sol gel method	UV irradiation	180	81	[39]
ZnO nanoparticle prepared by precipitate method	UV irradiation	180	92.5	[39]
Bioreduced ZnO nanoparticle	Sunlight	90	94.07	[40]
ZnO nanocrystalline	UV irradiation	100	99	[41]

reactions. In addition, a band gap in this range is commonly associated with rapid electron–hole recombination, causing many charge carriers to recombine before participating in surface redox processes. These factors collectively hinder the overall photocatalytic activity of porous ZnO [42]. In addition, the morphology and porosity of ZnO also play an important role in determining photocatalytic activity. The porous architecture generally increases surface area and enhances dye adsorption, which can facilitate a higher interaction frequency between methylene blue molecules and active sites. These enhanced interactions lead to improved photocatalytic performance [43]. However, despite this morphological advantage, the limited photon absorption and high recombination rate remain dominant factors constraining photocatalytic efficiency of the porous ZnO synthesized in this work.

4 Conclusions

Porous ZnO was successfully synthesized using carbon microspheres as templates. The template-assisted method enabled the formation of porous ZnO morphology with reduced crystallite size, uniform elemental distribution, enhanced textural properties (surface area, total pore volume, and pore size), and slightly narrower band gap (3.17 eV) compared to ZnO Ref. The photocatalytic tests showed that the degradation efficiency of porous ZnO against methylene blue increased with UV irradiation time, reaching the highest value 39.3 ± 0.2% at 150 min with a kinetic constant of 0.0032 ± 0.0001 min^{-1}. This study provides valuable insight into the use of carbon microspheres as a sustainable and effective template for producing porous ZnO. Although the photocatalytic efficiency is modest, the findings establish a basis for future optimization.

Acknowledgments

This research was supported by internal funding from Politeknik AKA Bogor program in 2024.

References

[1] Dardouri, S., Sghaier, J. "Adsorptive removal of methylene blue from aqueous solution using different agricultural wastes as adsorbents", Korean Journal of Chemical Engineering, 34(4), pp. 1037–1043, 2017. https://doi.org/10.1007/s11814-017-0008-2

[2] Tolkou, A. K., Giannoulaki, A., Chalkidi, P., Arvaniti, E., Fykari, S., Kritaki, S., Kyzas, G. Z. "Removal of Anionic and Cationic Dyes from Wastewater by Tetravalent Tin-Based Novel Coagulants", Processes, 13(7), 2103, 2025. https://doi.org/10.3390/pr13072103

[3] Khan, I., Saeed, K., Zekker, I., Zhang, B., Hendi, A. H., …, Khan, I. "Review on Methylene Blue: Its Properties, Uses, Toxicity and Photodegradation", Water, 14(2), 242, 2022. https://doi.org/10.3390/w14020242

[4] Ahmadi, B., Fallah, A., Ghamarpoor, R., Jamshidi, M. "Methylene blue beyond the dye: A critical review on its role as a benchmark pollutant in photocatalyst design", Results in Chemistry, 18, 102910, 2025. https://doi.org/10.1016/j.rechem.2025.102910

[5] Oladoye, P. O., Ajiboye, T. O., Omotola, E. O., Oyewola, O. J. "Methylene blue dye: Toxicity and potential elimination technology from wastewater", Results in Engineering, 16, 100678, 2022. https://doi.org/10.1016/j.rineng.2022.100678

[6] Karcıoğlu Karakaş, Z., Dönmez, Z. "A Sustainable Approach in the Removal of Pharmaceuticals: The Effects of Operational Parameters in the Photocatalytic Degradation of Tetracycline with MXene/ZnO Photocatalysts", Sustainability, 17(5), 1904, 2025. https://doi.org/10.3390/su17051904

[7] Chakravorty, A., Roy, S. "A review of photocatalysis, basic principles, processes, and materials", Sustainable Chemistry for the Environment, 8, 100155, 2024. https://doi.org/10.1016/j.scenv.2024.100155

[8] Danish, M. S. S., Estrella, L. L., Alemaida, I. M. A., Lisin, A., Moiseev, N., Ahmadi, M., Nazari, M., Wali, M., Zaheb, H., Senjyu, T. "Photocatalytic applications of metal oxides for sustainable environmental remediation", Metals, 11(1), 80, 2021. https://doi.org/10.3390/met11010080

[9] Kadem, A. J., Tan, Z. M., Suntharam, N. M., Pung, S. Y., Ramakrishnan, S. "Synthesis of CuO, ZnO and SnO_2 Coupled TiO_2 Photocatalyst Particles for Enhanced Photodegradation of Rhodamine B Dye", Bulletin of Chemical Reaction Engineering & Catalysis, 18(3), pp. 506–520, 2023. https://doi.org/10.9767/bcrec.19532

[10] Shu, X. "Research on Photoelectric Properties of ZnO-based Semiconductor Material", Journal of Physics: Conference Series, 2541(1), 012060, 2023. https://doi.org/10.1088/1742-6596/2541/1/012060

[11] Zhu, C., Wang, X. "Nanomaterial ZnO Synthesis and Its Photocatalytic Applications: A Review", Nanomaterials, 15(9), 682, 2025. https://doi.org/10.3390/nano15090682

[12] John Peter, I., Praveen, E., Vignesh, G., Nithiananthi, P. "ZnO nanostructures with different morphology for enhanced photocatalytic activity", Materials Research Express, 4(12), 124003, 2017. https://doi.org/10.1088/2053-1591/aa9d5d

[13] Revathi, G., Sangari, N. U., "Morphology dependent photocatalytic efficiency of nano ZnO towards Azure A dye", Open Ceramics, 16, 100465, 2023. https://doi.org/10.1016/j.oceram.2023.100465

[14] Chang, J. S., Saint, C. P., Chow, C. W. K., Bahnemann, D. W., Chong, M. N. "Recent innovations in engineering Zinc Oxide (ZnO) nanostructures for water and wastewater treatment: Pushing the boundaries of multifunctional photocatalytic and advanced biotechnological applications", International Materials Reviews, 69(7–8), pp. 337–379, 2024. https://doi.org/10.1177/09506608241280421

[15] Henriques Ferreira, S., Rovisco, A., dos Santos, A., Águas, H., Igreja, R., Barquinha, P., Fortunato, E., Martins, R. "Porous ZnO Nanostructures Synthesized by Microwave Hydrothermal Method for Energy Harvesting Applications", In: Ameen, S., Shaheer Akhtar, M., Shin, H.-S. (eds.) Nanopores, IntechOpen, 2021. ISBN 978-1-83880-209-7 https://doi.org/10.5772/intechopen.97060

[16] Mondal, K., Islam, M., Singh, S., Sharma, A. "Fabrication of High Surface Area Microporous ZnO from ZnO/Carbon Sacrificial Composite Monolith Template", Micromachines, 13(2), 335, 2022. https://doi.org/10.3390/mi13020335

[17] Zhu, S., Zhao, N., Li, J., Deng, X., Sha, J., He, C. "Hard-template synthesis of three-dimensional interconnected carbon networks: Rational design, hybridization and energy-related applications", Nano Today, 29, 100796, 2019. https://doi.org/10.1016/j.nantod.2019.100796

[18] Li, H., Wang, L., Wei, Y., Yan, W., Feng, J. "Preparation of Templated Materials and Their Application to Typical Pollutants in Wastewater: A Review", Frontiers in Chemistry, 10, 882876, 2022. https://doi.org/10.3389/fchem.2022.882876

[19] Lou, Z., Wang, Y., Yang, Y., Wang, Y., Qin, C., Liang, R., Chen, X., Ye, Z., Zhu, L. "Carbon sphere template derived hollow nanostructure for photocatalysis and gas sensing", Nanomaterials, 10(2), 378, 2020. https://doi.org/10.3390/nano10020378

[20] Kovács, Z., Márta, V., Gyulavári, T., Ágoston, Á., Baia, L., Pap, Z., Hernadi, K. "Noble metal modified (002)-oriented ZnO hollow spheres for the degradation of a broad range of pollutants", Journal of Environmental Chemical Engineering, 10(3), 107655, 2022. https://doi.org/10.1016/j.jece.2022.107655

[21] Wang, Y., Hu, K., Yang, Z., Ye, C., Li, X., Yan, K. "Facile Synthesis of Porous ZnO Nanoparticles Efficient for Photocatalytic Degradation of Biomass-Derived Bisphenol A Under Simulated Sunlight Irradiation", Frontiers in Bioengineering and Biotechnology, 8, 616780, 2021. https://doi.org/10.3389/fbioe.2020.616780

[22] Weldegebrieal, G. K. "Synthesis method, antibacterial and photocatalytic activity of ZnO nanoparticles for azo dyes in wastewater treatment: A review", Inorganic Chemistry Communications, 120, 108140, 2020. https://doi.org/10.1016/j.inoche.2020.108140

[23] Eswaran, P., Madasamy, P. D., Pillay, K., Brink, H. "Sunlight-driven photocatalytic degradation of methylene blue using ZnO/biochar nanocomposite derived from banana peels", Biomass Conversion and Biorefinery, 15(8), pp. 12347–12367, 2025. https://doi.org/10.1007/s13399-024-05999-z

[24] Krstić, S. S., Čokeša, Đ., Vujasin, R. T., Kaluđerović, B. V., Momčilović, M. Z. Jaćimovski, D., Gurikov, P., Dodevski, V. M. "Performance Analysis of Effective Methylene Blue Immobilization by Carbon Microspheres Obtained from Hydrothermally Processed Fructose", Processes, 12(12), 2683, 2024. https://doi.org/10.3390/pr12122683

[25] Zhang, Y., Hou, W., Guo, H., Shi, S., Dai, J. "Preparation and Characterization of Carbon Microspheres From Waste Cotton Textiles By Hydrothermal Carbonization", Journal of Renewable Materials, 7(12), pp. 1309–1319, 2019. https://doi.org/10.32604/jrm.2019.07884

[26] Wang, Y., Cui, L., Cheng, G., Yuan, N., Ding, J., Pesika, N. S. "Water-Based Lubrication of Hard Carbon Microspheres as Lubricating Additives", Tribology Letters, 66(4), 148, 2018. https://doi.org/10.1007/s11249-018-1102-2

[27] Liu, J., Li, R., Yang, B. "Carbon Dots: A New Type of Carbon-Based Nanomaterial with Wide Applications", ACS Central Science, 6(12), pp. 2179−2195, 2020. https://doi.org/10.1021/acscentsci.0c01306

[28] Yang, M., Su, J., Fang, C., Cheng, Y., Li, Y., Yan, Y., Lei, W. "Synthesis and Properties of Carbon Microspheres from Waste Office Paper", Molecules, 28(15), 5756, 2023. https://doi.org/10.3390/molecules28155756

[29] Mehmood, S. Z., Arshad, M., Alharbi, F. M., Eldin, S. M., Galal, A. M. "Multiferroics Made via Chemical Co-Precipitation That Is Synthesized and Characterized as $Bi_{(1-x)}Cd_xFeO_3$", Inorganics, 11(3), 134, 2023. https://doi.org/10.3390/inorganics11030134

[30] Kumari, H., Sonia, Suman, Ranga, R., Chahal, S., …, Parmar, R. "A Review on Photocatalysis Used For Wastewater Treatment: Dye Degradation", Water, Air, & Soil Pollution, 234(6), 349, 2023. https://doi.org/10.1007/s11270-023-06359-9

[31] Tu, N., Nguyen, K. T., Trung, D. Q., Tuan, N. T., Nam Do, V., Huy, P. T. "Effects of carbon on optical properties of ZnO powder", Journal of Luminescence, 174, pp. 6–10, 2016. https://doi.org/10.1016/j.jlumin.2016.01.031

[32] Parvaz, S., Rabbani, M., Rahimi, R. "Fabrication of novel magnetic ZnO hollow spheres/pumice nanocomposites for photodegradation of Rhodamine B under visible light irradiation", Materials Science and Engineering: B, 263, 114863, 2021. https://doi.org/10.1016/j.mseb.2020.114863

[33] Kyriakopoulos, G. L., Tsimnadis, K., Sebos, I., Charabi, Y. "Investigating the Effect of Pore Size Distribution on the Sorption Types and the Adsorption-Deformation Characteristics of Porous Continua: The Case of Adsorption on Carbonaceous Materials, Crystals, 14(8), 742, 2024. https://doi.org/10.3390/cryst14080742

[34] Satyam, S., Patra, S. "Innovations and challenges in adsorption-based wastewater remediation: A comprehensive review", Heliyon, 10(9), e29573, 2024. https://doi.org/10.1016/j.heliyon.2024.e29573

[35] Escobedo-Morales, A., Ruiz-López, I. I., Ruiz-Peralta, M. de L., Tepech-Carrillo, L., Sánchez-Cantú, M., Moreno-Orea, J. E. "Automated method for the determination of the band gap energy of pure and mixed powder samples using diffuse reflectance spectroscopy", Heliyon, 5(4), e01505, 2019. https://doi.org/10.1016/j.heliyon.2019.e01505

[36] Julita, M., Shiddiq, M., Khair, M. "Determination of Band Gap Energy of ZnO/Au Nanoparticles Resulting in Laser Ablation in Liquid", Indonesian Journal of Chemical Research, 10(2), pp. 83–87, 2022. https://doi.org/10.30598//ijcr.2022.10-mar

[37] Modwi, A., Ghanem, M. A., Al-Mayouf, A. M., Houas, A. "Lowering energy band gap and enhancing photocatalytic properties of Cu/ZnO composite decorated by transition metals", Journal of Molecular Structure, 1173, pp. 1–6, 2018. https://doi.org/10.1016/j.molstruc.2018.06.082

[38] Vallejo, W., Cantillo, A., Díaz-Uribe, C. "Improvement of the photocatalytic activity of ZnO thin films doped with manganese", Heliyon, 9(10), e20809, 2023. https://doi.org/10.1016/j.heliyon.2023.e20809

[39] Balcha, A., Yadav, O. P., Dey, T. "Photocatalytic degradation of methylene blue dye by zinc oxide nanoparticles obtained from precipitation and sol-gel methods", Environmental Science and Pollution Research, 23(24), pp. 25485–25493, 2016. https://doi.org/10.1007/s11356-016-7750-6

[40] Venkatesan, S., Suresh, S., Ramu, P., Arumugam, J., Thambidurai, S., Pugazhenthiran, N. "Methylene blue dye degradation potential of zinc oxide nanoparticles bioreduced using *Solanum trilobatum* leaf extract", Results in Chemistry, 4, 100637, 2022. https://doi.org/10.1016/j.rechem.2022.100637

[41] Priyadharshini, S. S., Shubha, J. P., Shivalingappa, J., Adil, S. F., Kuniyil, M., Hartshan, M. R., Shaik, B., Kavalli, K. "Photocatalytic Degradation of Methylene Blue and Metanil Yellow Dyes Using Green Synthesized Zinc Oxide (ZnO) Nanocrystals", Crystals, 12(1), 22, 2022. https://doi.org/10.3390/cryst12010022

[42] Zango, Z. U., Garba, A., Shittu, F. B., Imam, S. S., Haruna, A., …, Hosseini-Bandegharaei, A. "A state-of-the-art review on green synthesis and modifications of ZnO nanoparticles for organic pollutants decomposition and CO_2 conversion", Journal of Hazardous Materials Advances, 17, 100588, 2025. https://doi.org/10.1016/j.hazadv.2024.100588

[43] Alkhaldi, H., Alharthi, S., Alharthi, S., AlGhamdi, H. A., AlZahrani, Y. M., …, Abaza, S. F. "Sustainable polymeric adsorbents for adsorption-based water remediation and pathogen deactivation: a review", RSC Advances, 14(45), pp. 33143–33190, 2024. https://doi.org/10.1039/d4ra05269b